# Measuring Extended Structure in Stars using the Keck Interferometer Nuller

Chris Koresko[a] M. Mark Colavita[b] Eugene Serabyn[b] Andrew Booth[b] and Jean Garcia[b]

[a]Michelson Science Center, IPAC, Caltech, Pasadena, CA 91125, USA;
[b]Jet Propulsion Laboratory, Caltech, Pasadena, CA 91109, USA

## ABSTRACT

The Keck Interferometer Nuller is designed to detect faint off-axis mid-infrared light a few tens to a few hundreds of milliarcseconds from a bright central star. The starlight is suppressed by destructive combination along the long (85 m) baseline, which produces a fringe spacing of 25 mas at a wavelength of 10 $\mu$m, with the central null crossing the position of the star. The strong, variable mid-infrared background is subtracted using interferometric phase chopping along the short (5 m) baseline. This paper presents an overview of the observing and data reduction strategies used to produce a calibrated measurement of the off-axis light. During the observations, the instrument cycles rapidly through several calibration and measurement steps, in order to monitor and stabilize the phases of the fringes produced by the various baselines, and to derive the fringe intensity at the constructive peak and destructive null along the long baseline. The data analysis involves removing biases and coherently demodulating the short-baseline fringe with the long-baseline fringe tuned to alternate between constructive and destructive phases, combining the results of many measurements to improve the sensitivity, and estimating the part of the null leakage signal which is associated with the finite angular size of the central star. Comparison of the results of null measurements on science target and calibrator stars permits the instrumental leakage - the "system null leakage" - to be removed and the off-axis light to be measured.

**Keywords:** Nulling Interferometry, High-Contrast Imaging, Exozodiacal Dust

## 1. INTRODUCTION

The detection of faint objects near bright stars is one of the fundamental challenges of modern observational astronomy. Recent years have seen the development of a number of innovative approaches for improving the available contrast with single-telescope instruments, including classical Lyot coronagraphs behind adaptive optics (AO) systems,[1] coronagraphs which rely on image-plane phase masks[2,3] or novel amplitude mask designs,[4,5] speckle holography,[6] and differential imaging in two or more optical passbands.[7] Nulling interferometry has been used successfully with single telescopes.[8] Long baseline optical interferometry naturally produces very high angular resolution, and several approaches have been proposed to improve the dynamic range of interferometric measurements. These include differential phase[9] and nulling[10,11] .

Here we present a description of the first long-baseline nulling instrument working at infrared wavelengths, and some early results on the sky. We begin in section 2 with a discussion of the fundamental principles of nulling interferometry, and the practical challenges it presents, and simplified approaches to dealing with those challenges. In section 3 we describe the methods used to produce stable, high-quality wavefronts as inputs to the beam combiner. The nulling beam combiner itself is described in section 4, and the measurement of the fringes it produces is described in section 5. The data reduction algorithms are described in section 6. Finally, in section 7 we show results from some early measurements on the sky.

Send correspondence to C. Koresko at koresko@ipac.caltech.edu or (818) 354 6680

## 2. PRINCIPLES OF LONG-BASELINE NULLING INTERFEROMETRY

Long-baseline nulling interferometry relies on the destructive combination in the pupil plane of light from two or more telescope apertures to selectively suppress unwanted light from an on-axis source such as a bright star, while allowing off-axis light to reach the detector. Nulling can be regarded as a form of coronagraphy in which a central dark fringe ("null") plays the role of the image-plane spot. Note that no image is produced; the detected signal is the integral of the product of the light intensity on the sky and the instrumental response pattern ("beam").

### 2.1. The Single-Baseline Nuller

The response pattern on the sky for a two-aperture, single-baseline nuller is shown schematically in Figure 1. The outer envelope is defined by the beam of a single telescope aperture, here assumed to be a filled circle. This envelope is crossed by a set of fringes produced by interference between the light from the two apertures. The fringe phase corresponds to the shift of the central bright fringe from the center of the envelope. If the central star lies in a dark fringe, its contribution will be suppressed relative to that of a companion star or disk which lies outside the null.

The science measurement is the fraction of the total starlight which leaks through the null. This leakage is the sum of several components associated with the instrument and with the target star. In the case of a single-baseline nulling beam combiner, these terms depend quadratically on small deviations from an ideal system in which wavefront aberrations, fringe phase errors, input intensity imbalances, polarization rotation, birefringence, and the angular size of the target star all vanish.[12] In these terms, we are interested in the ones associated with the photosphere of the star and any surrounding material, e.g., a stellar or substellar companion or a dust disk. The instrumental terms must be calibrated out using either auxiliary data which describe the instrument performance and/or observations of calibrator stars.

A hypothetical nulling experiment using a single-baseline instrument might proceed as follows: with the null fringe centered on the bright star, measure the flux at the detector. Then adjust the fringe phase by $\pi$ radians, i.e., from the null to the constructive peak using, e.g., a delay line. The null leakage would be the ratio of the nulled flux to the peak flux.

In practice, such an experiment would likely not produce a useful measurement when carried out at mid-infrared wavelengths using a ground-based instrument. One reason is that the thermal infrared emission produced by the telescopes and any other warm optics in the beamtrain contribute a poorly known background flux which would be added to the starlight signal. In addition, the atmosphere produces a significant background whose fluctuations exceed the shot noise of the background for frequencies below about 10 Hz,[13] severely limiting the sensitivity of a staring measurement of any but the brightest stars. Thus both the null and peak fluxes would suffer from large and unknown background offsets, making their ratio poorly determined.

The traditional solution for single-aperture photometry in the mid-infrared is to modulate the telescope beam position (e.g., by wobbling the secondary mirror) so that the star falls alternately in and out of the beam. This causes the starlight to be modulated with a known frequency and phase, while ideally the background light exhibits no correlated changes, and thus the starlight signal can be detected with good sensitivity via coherent demodulation (e.g., using a lock-in amplifier). In principle this technique could be applied to the single-baseline nuller as well. However, the demands on the modulating optics would be relatively severe: the starlight flux through the two apertures would need to be sufficiently accurately matched to permit effective cancellation of the starlight. In addition, if the moving optic were more than a few surfaces downstream of the primary mirror, as is likely to be convenient for a long-baseline interferometer, then the optical path for the starlight would move on the surface of the primary and any intermediate optics, resulting in a modulation of the thermal background at the same frequency and biasing the demodulated starlight signal. For single-telescope measurements this bias effect is traditionally corrected by guiding the telescope so that the star falls alternately into each of the two chop beams, and forming the difference of the demodulated signals in these two states. But the photometric precision of such observations is normally limited to a few percent of the starlight flux, which is not sufficient for many of the science goals which nulling is intended to address.

### 2.2. The Four-Baseline Nuller

The above limitations of the single-baseline nulling interferometer led us to adopt a more complicated four-aperture, four-baseline design for the Keck Interferometer Nuller (KIN). This system has two parallel long (85 m) baselines and two parallel short (5 m) baselines (see Figure 2). The nulling fringes are formed on the long baselines. The short baselines produce an additional broad set of interference fringes. These are shown schematically in Figure 2 for a nominal orientation of the short baselines perpendicular to the long ones. For KIN, the four apertures required are produced by optically bisecting each 10 m Keck telescope pupil.

The expected angular size of the extended structure being studied is presumed to be intermediate between the widths of the broad and narrow fringes. Therefore, a shift in the phase of the broad fringes will modulate the light from the entire astrophysical source, including light leaking through the central null and any structure extending beyond it, without affecting the incoherent background light. By dithering the optical path difference (OPD) of the short baseline by one wavelength, at a frequency faster than the fluctuations of the thermal infrared background, we can simulate the effect of a chopping secondary. The detected signal is then demodulated using a software lock-in amplifier. We refer to this technique as "interferometric chopping". It brings several advantages over the traditional chopping secondary, some obvious and some subtle. First, because there is no angular displacement of any optic at the frequency of the starlight modulation, the problem of the bias due to beamwalk is eliminated. Second, the OPD modulation requires only piston motion of a small mirror by about half a wavelength, so it can readily be implemented precisely and at a high frequency.

More subtly, the sensitivity of the demodulated leakage signal to some of the error terms changes to a more desirable form in a four-baseline system such as KIN. In particular, while the dependence of the leakage through the null on the phase and input intensity errors have quadratic forms in the unmodulated single-baseline case, in the four-baseline case it can be shown that the equivalent demodulated terms are proportional to products of the phase and intensity errors, respectively, along the long baselines:

$$N_{amp} = \frac{1}{4}\alpha_0\alpha_1 \tag{1}$$

$$N_{\phi} = \frac{1}{4}\beta_0\beta_1 \tag{2}$$

where the $\alpha_i$ and $\beta_i$ are the relative wavefront amplitude errors and phase errors, respectively, along the two long baselines. In the limit that these errors are driven by the servos to be zero-mean, uncorrelated, rapidly changing random numbers, they contribute only zero-mean noise to the time-averaged leakage.

Schematically, the experiment design for the four-baseline case is not very different from its single-baseline counterpart. In principle it should be possible to obtain a more accurate null leakage measurement with the four-baseline system. The hypothetical measurement is still the ratio of the signal with the long baselines tuned to null to the same signal when they are tuned to the constructive peak. However, the signals involved are now demodulated with respect to the modulation of the phase of the short-baseline fringe, and the thermal background is "chopped out" in a way which is in principle essentially bias-free. In the following section we discuss some other factors which complicate the experiment, and the approaches taken to deal with them for KIN.

## 3. PRODUCING GOOD WAVEFRONTS

The above simplified description assumes that the mid-infrared fringes are produced with stable, high-quality wavefronts with matched intensities and which do not suffer longitudinal dispersion or differential polarization. Producing such wavefronts in the presence of Earth rotation, atmospheric seeing and the imperfections of real optics, and instrument vibrations is nontrivial. Here we briefly summarize the steps used to produce them for KIN.

The raw atmospheric wavefronts seen by the two telescopes typically correspond to relatively low Strehl ratios, even in the mid-infrared. This necessitates the use of adaptive optics (AO). For KIN, each Keck telescope

is equipped with an AO system whose wavefront sensor operates at visible wavelengths.[15] The Strehl ratio at 2 $\mu$m is typically of the order of 0.5, corresponding to wavefront errors of the order of a few hundred nm, corresponding to a Strehl ratio of around 0.97 at 10 $\mu$m.

The infrared light is selected by a dichroic mirror and sent to a Dual-Star Module (DSM) which bisects the corrected wavefront in the pupil plane and passes the infrared light in each resulting subaperture to a passive Long Delay Line (LDL; in practice, each LDL mechanism is large enough to carry two separate beams). The light emerging from each LDL is then separated into long (mid-infrared; MIR) and short (near-infrared; NIR) wavelength beams, resulting in a total of eight beams. Each of these is sent to a Fast Delay Line (FDL). The FDLs are actively controlled; it is these devices which are used to fine-tune the optical path difference (OPD) to adjust the phase of the fringes along the long baselines.

The reason for segregating the near and mid infrared light is to permit use of the NIR as a high-SNR proxy for the MIR phase and tilt. The background light at NIR wavelengths is much smaller than in the MIR, and NIR detectors tend to have much lower readnoise, so the photometric SNR is much higher in the NIR than in the MIR. This is important because it allows the NIR fringe-tracking servos to operate at the higher frequencies (tens of Hz) necessary to follow the phase disturbances due to atmospheric seeing.

The NIR beams are further split into short ($< 2.0$ $\mu$m) and long ($> 2.0$ $\mu$m) regions. The short-wavelength beams go to narrow-angle cameras (the "Keck Angle Trackers", or KATs) which are used to monitor the tilt of the beams close to the beam-combiners. The positions measured by the KATs are used to drive fast tip-tilt mirrors which stabilize the beam tilts. The tilt information is fed forward into the MIR beams, which are expected to suffer similar tilts because they share long common paths.

The longer wavelength beams go to NIR fringe trackers ("FATCATs") which monitor the fringe phases along the long baselines.[14] The FATCATs contain low-resolution spectrometers which allow them to provide information about the longitudinal dispersion as well as the broadband fringe position. These quantities can be used to compute water vapor and "dry air" differential columns, and knowledge of them in the NIR provides good estimates for their effects in the MIR, with the exception of slow drifts.[16–18] Additional phase information at high temporal frequencies is derived from accelerometers on the telescope mirrors and structures, and from laser metrology along the beamtrain. The actual FDL positions for the MIR beams are controlled by the metrology and accelerometer measurements at high temporal frequencies and by the MIR phase measurements themselves at low frequencies.

The longitudinal dispersion in the MIR is controlled by an Atmospheric Dispersion Controller (ADC) in each Nuller input beam. The ADC optics consist of pairs of matched, opposed ZnSe wedges.[18] The choice of ZnSe was made after an exhaustive search of a catalog of infrared materials. It offers a good fit to the refractivity of air over a usefully broad region of the MIR, is non-hygroscopic, has good transmission in the MIR and offers useful transmission at visible wavelengths, and is readily available. The wedges are right triangles with their hypotenuse faces facing each other. One wedge of each pair is actuated and translates along an axis perpendicular to the opposed faces, so that the dispersion controller can be thought of to first order as a plane-parallel glass plate of adjustable thickness. Beams passing through an ADC suffer no net angular dispersion, a lateral translation, and only a small lateral dispersion. The net dispersion along each baseline can be adjusted about zero. The ADC positions are encoded and their OPD contributions are fed back to the FDLs, so that from a control perspective the OPD and dispersion become orthogonal, i.e., one can adjust the dispersion and OPD independently.

An important subtlety arises from the fact that the dispersion due to the offset from the central fringe changes in increments for successive fringes. For each fringe there is an optimum combination of ADC and FDL settings which minimize the RMS wavelength-dependent phase error. As currently implemented, the dispersion control servo system monitors only the linear term, i.e., the slope of the phase as a function of wavelength, and is unable to choose the best fringe for itself. Instead, the choice is made *a priori* according to the differential air pathlength and the humidity measured at several points along the beamtrain.

The beamtrain and the Nuller are achromatized together at zero OPD using retroreflected light from a thermal source in the beam-combining lab. The procedure is to obtain a set of Fourier Transform Spectra (FTS) scans, from which the residual refractivity is derived along with the spectrometer channel wavelengths. The refractivity is fitted with a model consisting of a non-dispersive OPD and an adjustable thickness of ZnSe. The model is

optimized for each of a series of fringes, and the parameters for the best fringe are applied to the ADCs. This procedure is done frequently (typically a few times per observing run) for the MMZs, and less frequently (every few observing runs) for the XCs. It provides a sensible starting point for servo tracking of the dispersion.

There is currently no explicit control of polarization for KIN. However, the contribution of polarization effects to the null leakage is expected to be modest due to careful choices of optical materials, e.g., bare gold coatings instead of overcoated silver for optics working at non-normal incidence.

## 4. OPTICAL CONFIGURATION OF THE NULLER

The MIR light from the four beams is combined in the pupil plane by the nulling beam combiner.[19] This somewhat complicated optical system can be regarded to first order as simply adding the amplitudes of the input beams, and sending the combined output through a beamsplitter to two (four, once development of the instrument is complete) outputs. In practice this combination is done in two distinct stages, with the two long baselines being combined first in pair of separate modified Mach-Zehnder (MMZ) combiners whose symmetric outputs go to a simple Michelson-type "cross-combiner" (XC) which amounts to a 50-50 beamsplitter and a compensator plate. The MMZ design provides a high degree of symmetry in the sense that the light reaching its symmetric output beams from each of the inputs encounters the same number of reflections and transmissions, at the same angles, and the same thickness of substrate material. In addition, care was taken to match the performance of the optical components by having them coated together. This symmetry helps minimize any loss of fringe contrast due to the Nuller optics. The demodulated null leakage is less sensitive to the quality of the combination along the short baselines, permitting the simpler Michelson design to be used for the XCs.

## 5. FRINGE MEASUREMENT AND TRACKING IN THE MIR

Each Nuller output goes to one input port of a low-resolution MIR spectrometer, called KALI.[20] Each input beam is conditioned by an AO system, a tip-tilt stabilizer, a dispersion controller, and an intensity controller. In addition, each beam has a "switching" mirror which is used as a fast shutter (it steers the beam enough to prevent it from reaching the detector in the "off" state). This switching ability is used to allow the fringes along individual baselines to be examined without interference from the additional beams.

Measurement of the fringe amplitude and phase in the MIR with the KALI spectrometer is done the same way as for the NIR. Briefly, four detector reads are taken while the FDL moves the OPD through one wavelength. These four reads, which we refer to as *A,B,C,* and *D*, are used to compute fringe quadratures. These are sufficient to derive both the phase and amplitude of the fringe.[21] As for the NIR case, an additional *Z* read is taken but ignored. This is to provide dead time for FDL flyback and switching mirror motions.

Nulling measurements require the quasi-simultaneous monitoring and control of the phases and group delays of three MIR fringes, namely those produced by the two long baselines plus one produced by the short baseline (the phase and group delay for the two short baselines are degenerate). As of April 2006, this is implemented by cycling rapidly through a set of four modes: two for measuring the fringes for the two MMZs, respectively; one for measuring the signal with both MMZ phases adjusted to null (i.e., the Null signal); and a corresponding measurement made with the MMZ phases adjusted to their constructive peaks (i.e., the Peak signal). This "gated servo cycle" occurs on a 200 msec timescale, which is shorter than the filter length for the MIR phase and group delay measurements, so those measurements can be regarded as continuous from the point of view of the servos. These long filter lengths are practical because information about the rapid fringe motions is derived from the metrology systems, accelerometers, and the NIR fringe trackers, as described above.

The XC fringe phase is dithered over $2\pi$ at a rate of 0.1 Hz. This offers two advantages. First, the contribution of any static bias quadrature to the XC signal vanishes when averaged over one wavelength of this modulation. The modulation also reduces the effect of any cyclic error in the phase estimator.

For measuring an MMZ phase, the two inputs to the other MMZ are switched off using the switching mirrors, and one of the FDLs of the active MMZ is dithered by a wavelength. The measurements of the null and peak fringes are made by switching on all four input beams and applying identical dithers to the pathlengths of both inputs of one MMZ. This is implemented as motion of a single "rapid ramp" mirror downstream of the MMZ

where these two beams have already been combined, rather than simply dithering the appropriate pair of FDLs. The reason for this is to permit more precise matching of the dither patterns.

## 6. DATA ANALYSIS

The reduction of nulling data to prepare it for astrophysical modeling takes place in two steps, which we refer to as "Level 1" and "Level 2" (the raw data are referred to as "Level 0"). The Level 1 reduction consists of steps which are *internal* in the sense that they rely on information derived from a single visit to a star. They can account for a subset of the terms contributing to the overall leakage through the null, such as phase and amplitude errors in the MMZs. The Level 1 reduction also includes time-averaging the data taken during a visit.

The Level 2 reduction is intended to account for those leakage terms which cannot be measured directly from the science target. Those terms, such as those due to polarization, optical misalignment, and wavefront corrugation, contribute a *system leakage* which must be determined empirically. In practice, the system null leakage is measured by observing a calibration source of a known effective angular diameter, and subtracting the diameter leakage term from the observed total leakage measured for that source. The system leakage is implicitly assumed to vary slowly with time (i.e., it is well correlated on a timescale longer than the time between science-target and calibrator-target observations, which is typically 15–30 minutes). It is also assumed to vary slowly with the telescope coordinates (altitude and azimuth), so that those effects will be small if the calibration target is near the science target in the sky.

Level 1 reduction proceeds in several distinct steps. The fringe quadratures suffer biases from, e.g., residual switching mirror motion outside the $Z$ read. These are measured by taking"foreground" data with the OPDs set to be outside the fringe envelopes and the phase tracking servos disabled. These quadrature biases are subtracted from the raw fringe quadratures. As for the NIR case, mismatch between the wavelength of a given spectral channel and the length of the OPD stroke is accounted for by a "dewarping" calibration. A further correction is made for detector "ripple", i.e., the apparent pixel-dependent phase shift produced by the differences between the readout timings for the various detector pixels. This ripple effect is significant since the KALI detector is read out continuously, so that the time between the reading of the first and last pixels is nearly equal to the frame time. The starlight for two of the input ports is dispersed perpendicular to the detector readout direction, and for those ports the delay between the first and last pixels in the spectrum corresponds to a phase shift of about 0.8 radians. Finally, an empirically determined phase offset is applied to convert the apparent fringe phase to the true phase. This latter step is necessary to account for small effects such as nonlinearity in the FDL stroke.

The XC fringe amplitudes for each 200 msec gated servo cycle are derived from the calibrated quadratures during the nulling and the peak modes. This involves coherently demodulating the fringe signal by projecting the {X,Y} quadratures onto a unit vector whose phase is determined from the phase of the XC signal with the MMZs tuned to constructive combination. For each visit to a science or calibration target, these quantities are averaged over 10 equal time spans. The null depth for each of these time spans is computed as the ratio of the signal at null to the signal at peak, and an internal errorbar is computed from the scatter among them with the assumption of Gaussian statistics.

The null leakage term due to MMZ phase errors is estimated as

$$L_\phi \simeq \frac{1}{4}\langle \beta_0 \beta_1 \rangle \tag{3}$$

where $\beta_0$ and $\beta_1$ are the phase errors of the two MMZs (measured in radians), respectively, and the angle brackets denote an average over all the measurements made during the visit. The approximation is valid when the $\beta$s are small compared to unity. In principle, one should be able to subtract this phase error leakage term from the observed null leakage in order to improve the accuracy of the final calibration. However, this has not turned out to work very well in practice, probably because our phase error measurements are not sufficiently well calibrated or precise on short timescales.

The Level 2 reduction corrects the leakage measurements on the science targets for the system leakage, in principle leaving only the leakage due to the astrophysics, i.e., the finite angular extent of the science target.

The first step is to derive the system leakage from each visit to a calibration target by subtracting the diameter leakage for that target from the observed total leakage. The diameter leakage for a uniform-disk star is[12]

$$L_{dia} \simeq \frac{\pi^2}{16} \left( \frac{\theta_{dia} B_{proj}}{\lambda} \right)^2 \tag{4}$$

where $\theta_{dia}$ is the angular diameter of the star, $B_{proj}$ is the length of the projected long baseline, and $\lambda$ is the observing wavelength. Tthe approximation is valid as long as the quantity in parenthesis is small compared to unity.

The system leakage derived from the various calibration star measurements is then interpolated to the times of the science target measurements. Subtracting the interpolated system leakage from the leakage measured on the science target gives the Level 2 calibrated leakage for the science target measurement. The science and calibration targets are typically visited several times during a night, with the visits interleaved so that the Level 2 calibrated data will be insensitive to slow drifts in the system leakage. If, as is typically the case, the change in the projected long baseline $B_{proj}$ is small during the course of these measurements, the calibrated leakages can be averaged. In practice, the average is weighted according to the internal errorbars, and an external errorbar is derived from the scatter between the leakage measurements.

### 6.1. Null Leakage vs. Visibility

It is worth noting that the null leakage $N \equiv \frac{I_{min}}{I_{max}}$, has a simple arithmetical relationship with the traditional interferometer visibility $V \equiv \frac{I_{max}-I_{min}}{I_{max}+I_{min}}$. Thus the nulling experiment can be regarded as equivalent to a visibility measurement.

The relationship is readily found to be

$$N = \frac{1-V}{1+V} \tag{5}$$

$$= 1 - 2V + 2V^2 - 2V^3 + ... \tag{6}$$

and similarly,

$$V = \frac{1-N}{1+N} \tag{7}$$

$$= 1 - 2N + 2N^2 - 2N^3 + ... \tag{8}$$

In the typical case for which $N \ll 1$ it is usually adequate to keep only the first-order term.

The quantity most commonly used to describe the result of a measurement by a long-baseline optical interferometer is the squared visibility $V^2$. This quantity can expressed in terms of the null leakage as

$$V^2 = 1 - 4N + 8N^2 - 12N^3 + ... \tag{9}$$

Its uncertainty is related to the uncertainty in the null leakage as

$$\sigma_{V^2} \simeq 4\sigma_N \tag{10}$$

when $N \ll 1$.

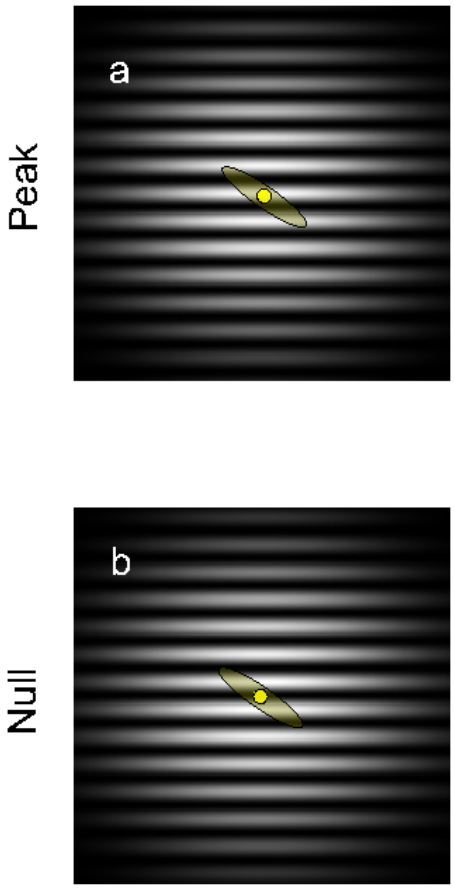


**Figure 1.** Fringes for a one-baseline nuller configuration. A schematic star+disk system is shown to illustrate the effect of the various fringe phases. The star is smaller than the spacing of the long-baseline fringes, while the size of the disk is large enough to extend well beyond the central null. Schematically, the measurement is the ratio of the flux detected when the star is nulled (1b) to the flux when the star lies on a fringe peak (1a).

## 7. NULLING EXPERIMENT RESULTS

Full Level 2 calibration of KIN data was tested in April 2006. The experiment consisted of observing two stars of similar brightness, effective temperature, and angular diameter (Chi UMa: N-band flux = 15 Jy, $\theta_{dia} = 3.35$ mas, $T_{eff} = 4380$ K; 3 CVn: N-band flux = 15 Jy, $\theta_{dia} = 3.34$ mas, $T_{eff} = 3690$ K) three times each, and arbitrarily choosing 3 CVn to play the role of the science target with Chi UMa as its calibration target. The measurements of the two stars were interleaved in time, and the time between successive measurements averaged around 15 minutes. Neither of these stars is expected to show significant extended flux above its photosphere, so the final Level 2 reduced null leakage should correspond to a uniform disk of the photospheric diameter of the science target.

The final null leakage is plotted as a function of wavelength in Figure 3. The data are consistent with the model. The broadband average over the 6 channels with center wavelengths between 8.5 and 10.5 $\mu$m, weighted according to their errorbars, is $0.013 \pm 0.002$. This is very close to the theoretical value of 0.0120. This 1-$\sigma$ Level 2 calibration precision corresponds to an error in the squared visibility $V^2$ of 0.7%.

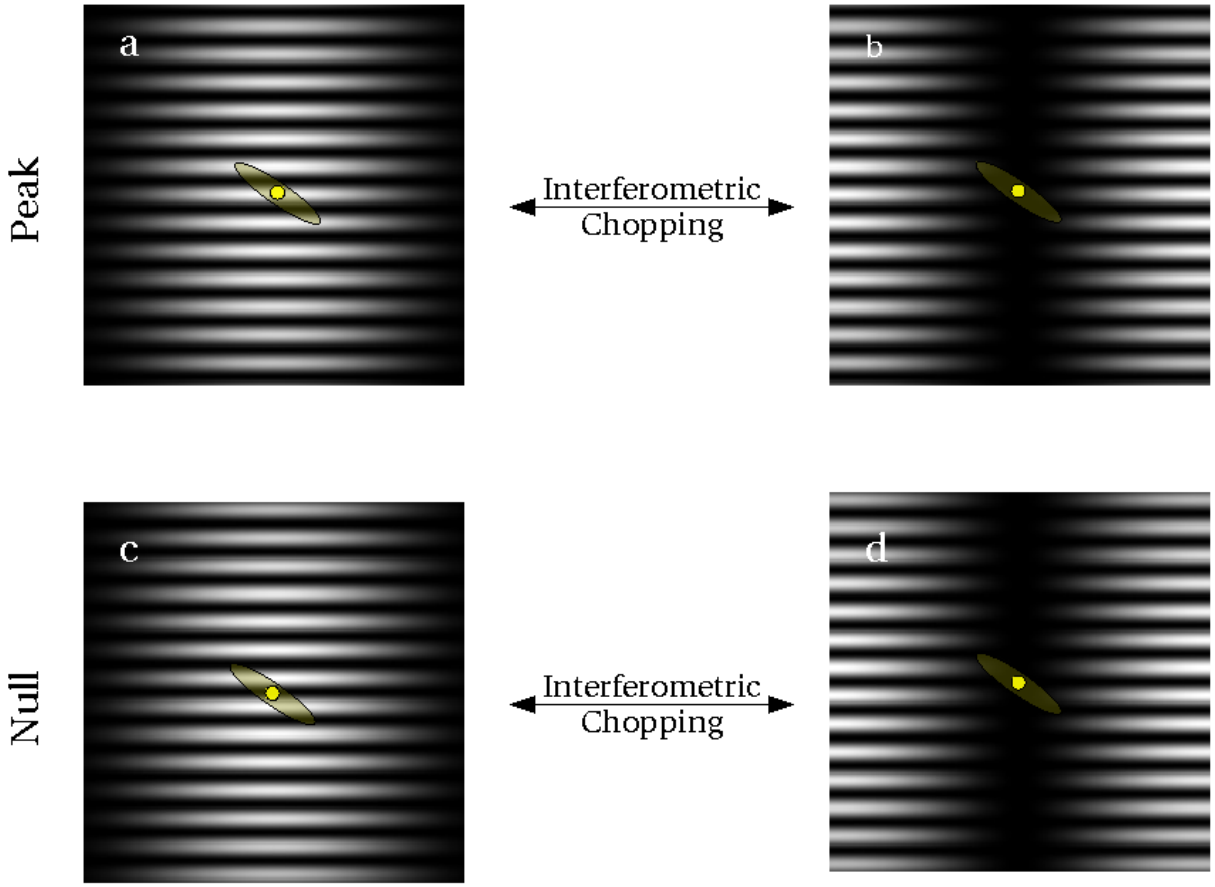


**Figure 2.** Fringes for a four-baseline nuller configuration in which the nulling is done on a pair of parallel long baselines. The short baseline produces a perpendicular set of broad fringes across the primary beam. Their phase is modulated at a rate fast enough to "chop out" the variations in the thermal background, a process we refer to as *interferometric chopping*. A schematic star+disk system is shown to illustrate the effect of the various fringe phases. The star is smaller than the spacing of the long-baseline fringes, while the size of the disk is intermediate between the spacings of the long and short baseline fringes. Figs 2a and 2b illustrate the measurement of the light from the central star, which is modulated by the movement of the short-baseline fringe. Figs 2c and 2d show the corresponding measurement of the disk, whose faint light is significant only because the starlight is suppressed by central null of the long-baseline fringe.

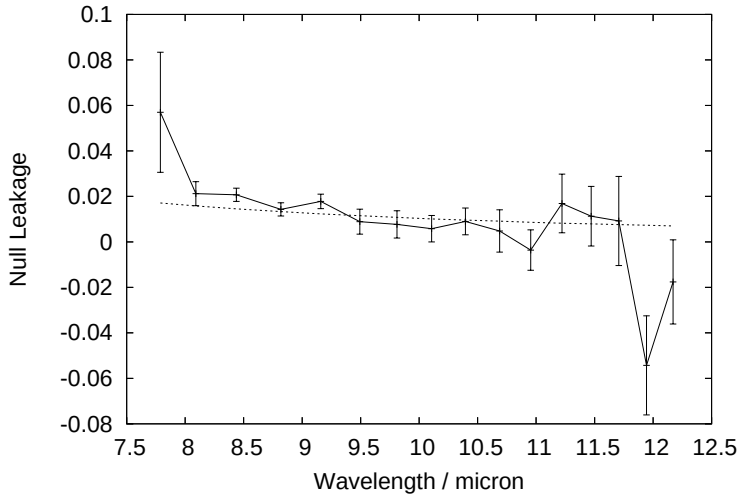


**Figure 3.** The level-2 calibrated null leakage for 3 CVn, with Chi UMa as a calibration target, is as a solid curve. The errorbars are computed from the scatter among the science target and calibration target measurements. The dotted curve is the leakage expected for a uniform disk the size of 3 CVn. The broadband null leakage is consistent with the astrophysical prediction. The consistency of the measured data with the prediction confirms that the instrument is successfully calibrated.

## ACKNOWLEDGMENTS

Funding was provided by NASA through the Keck Interferometer project. The W. M. Keck Observatory is operated as a scientific partnership among the California Institute of Technology, the University of California, and NASA. The Observatory was made possible by the generous Financial support of the W. M. Keck Foundation. The research presented here was conducted at the Jet Propulsion Laboratory, California Institute of Technology, and the Michelson Science Center, California Institute of Technology, under contract with the National Aeronautics and Space Administration. The authors wish to recognize and acknowledge the very significant cultural role and reverence that the summit of Mauna Kea has always had within the indigenous Hawaiian community. We are most fortunate to have the opportunity to conduct observations from this mountain.

## REFERENCES

1. A. Sivaramakrishnan, C.D. Koresko, R.B. Makidon, T. Berkefeld, & M.J. Kuchner "Ground-based Coronagraphy with High-order Adaptive Optics", *ApJ* **552**, 397, 2001
2. F. Roddier & C. Roddier "Stellar Coronograph with Phase Mask" *PASP* **109**, 815, 1997
3. D. Rouan, P. Riaud, A. Boccaletti, Y. Clenet, & A. Labeyrie "The Four-Quadrant Phase-Mask Coronagraph. I. Principle", *PASP*, **112**, 1479, 2000
4. R.J. Vanderbei, D.N. Spergetl, & N.J. Kasdin "Circularly symmetric apodization via star-shaped masks" *ApJ* **599**, 686, 2003
5. M.J Kuchner, J. Crepp, & J. Ge, "Eighth-order image masks for terrestrial planet finding" *ApJ* **628**, 466, 2005
6. A. Chelli "The phase problem in optical interferometry - Error analysis in the presence of photon noise" *A&A* **225**, 277, 1989
7. C. Marois, R. Racine, R. Doyon, D. Lafrenire, & D. Nadeau "Differential Imaging with a Multicolor Detector Assembly: A New Exoplanet Finder Concept" *ApJL* 615, 61, 2004
8. P.M. Hinz, J.R.P. Angel, W.F. Hoffman, D.W. McCarthy, P.C. McGuire, M. Cheselka, J.L. Hora, & N.J. Woolf "Imaging circumstellar environments with a nulling interferometer", *Nature* **395,** 251, 1998

9. R, Akeson & M. Swain "Differential Phase Observations of Extrasolar Planets with the Keck Interferometer" *ASPC* **212**, 300
10. R.N. Bracewell & R.H. MacPhie *Icarus* **38**, 136
11. M. Shao & M.M. Colavita *ARAA* **30**, 457
12. E. Serabyn "Nulling interferometry: symmetry requirements and experimental results" *Proc. SPIE* **4006**, 328, 2000
13. C.H. Smith, & D.A. Harper "Mid-infrared sky brightness site testing at the South Pole" *PASP* **110**, 747
14. G. Vasisht, A.J. Booth, M.M. Colavita, R.L. Johnson, E.R. Ligon, J.D. Moore, & D.L. Palmer "Performance and verification of the Keck interferometer fringe detection and tracking system" *SPIE* **4838**, 824, 2003
15. P. Wizinowich, D.S. Acton, C. Shelton, P. Stomski, J. Gathright, K. Ho, W. Lupton, & K. Tsubota "First Light Adaptive Optics Images from the Keck II Telescope : A New Era of High Angular Resolution Imagery" *PASP* **112**, 315
16. M.M. Colavita, M.R. Swain, R.L. Akeson, C.D. Koresko, & R.J. Hill, "Effects of Atmospheric Water Vapor on Infrared Interferometry" *PASP* **116**, 876
17. C.D. Koresko, M.M. Colavita, E. Serabyn, A. Booth, & J.I. Garcia "Water vapor measurement and compensation in the near- and mid-infrared with the Keck interferometer nuller" *Proc SPIE* (these proceedings)
18. C.D. Koresko, B.P. Mennesson, E. Serabyn, M.M. Colavita, R.L. Akeson, & M.R. Swain "Longitudinal dispersion control for the Keck interferometer nuller" *Proc. SPIE* **4838**, 625, 2003
19. S.L. Crawford, M.M. Colavita, J.I. Garcia, E.R. Ligon, B. Mennesson, C.G. Paine, E. Serabyn, R.F. Smythe, M.R. Swain, & G. Vasisht "Final laboratory integration and test of the Keck Interferometer nuller" *Proc SPIE* **5905**, 59050U-1, 2005
20. M.J. Creech-Eakman, J.D. Moore, D.L. Palmer, & E. Serabyn "KALI Camera: mid-infrared camera for the Keck Interferometer Nuller" *Proc SPIE* **4841**, 330, 2003
21. M.M. Colavita "Fringe Visibility Estimators for the Palomar Testbed Interferometer" *PASP* **111**, 111, 1999